ELSEVIER

International Journal of Heat and Fluid Flow 21 (2000) 92–103

International Journal of HEAT AND FLUID FLOW

www.elsevier.com/locate/ijhff

Effects of inner cylinder rotation on laminar flow of a Newtonian fluid through an eccentric annulus

M.P. Escudier [a,*], I.W. Gouldson [a], P.J. Oliveira [b], F.T. Pinho [c]

[a] *Department of Engineering, Mechanical Engineering, University of Liverpool, Brownlow Hill, Liverpool, L69 3GH, UK*

[b] *Departamento de Engenharia Electromecânica, Universidade de Beira Interior, Rua Marquês D'Ávila e Bolama, 6200 Covilhã, Portugal*

[c] *Faculdade de Engenharia, Centro de Estudos de Fenómenos de Transporte, DEMEGI, Universidade do Porto, Rua dos Bragas, 4050-123 Porto, Portugal*

Received 23 May 1999; accepted 10 August 1999

Abstract

The paper concerns a computational and experimental study of fully developed laminar flow of a Newtonian liquid through an eccentric annulus with combined bulk axial flow and inner cylinder rotation. The results are reported for calculations of the flowfield, wall shear stress distribution and friction factor for a range of values of eccentricity ε, radius ratio κ and Taylor number Ta. For fully developed flow the radial/tangential motion is decoupled from the axial component of velocity. However, the axial component of velocity is directly affected by the radial/tangential velocity field and rotation of the inner cylinder is found to have a strong influence on the axial velocity distribution, ultimately leading to two maxima in the case of a highly eccentred inner cylinder at high rotation speeds, a feature not reported hitherto. This influence of rotation on the axial velocity is mirrored in the behaviour of the shear stresses on the inner and outer cylinder walls and hence on the friction factor. An unexpected result is that (at fixed Reynolds number) as the Taylor number is increased the friction factor for high values of $\varepsilon(> 0.9)$ increases rather than decreases.

Keywords: Laminar; Newtonian; Annulus; Eccentric; Rotation

Notation

D_H	hydraulic diameter 2δ
e	displacement of inner cylinder axis from outer cylinder axis (m)
f	Fanning friction factor $-(\delta/\rho U^2)(\partial p/\partial z)$
f_0	value of f for $\omega = 0$
g	gap width (A, B, C or D)
p	pressure (Pa)
$\bar{p}$	non-dimensional pressure $p\delta/\mu\omega R_I$
Q	azimuthal flowrate (m^3/s)
r	radial distance from axis of inner cylinder (m)
$\bar{r}$	non-dimensional value of r, r/δ
R_I	outer radius of inner cylinder (m)
R_O	inner radius of outer cylinder (m)
Re	bulk axial Reynolds number $2\rho U\delta/\mu$
Ro	rotational Reynolds number $\rho\omega R_I^2/\mu$
T	rotational Reynolds number $\rho\omega R_I\delta/\mu$
Ta	Taylor number $(\rho\omega/\mu)^2 R_I\delta^3$
Ta_C	critical Taylor number
Ta_0	value of Ta_C for $\varepsilon = 0$
u	axial component of velocity (m/s)
$\bar{u}$	non-dimensional value of u, u/U
u_{max}	peak value of u in any sector of the annulus (m/s)
U	bulk axial velocity (m/s)
v	tangential component of velocity (m/s)
$\bar{v}$	non-dimensional value of v, $v/\omega R_I$
w	radial component of velocity (m/s)
$\bar{w}$	non-dimensional value of w, $w/\omega R_I$
y	distance from outer wall of inner cylinder (m)
$\bar{y}$	non-dimensional value of y, y/δ
z	axial distance (m)
δ	mean annular gap width $R_O - R_I$ (m)
ε	eccentricity e/δ
κ	radius ratio R_I/R_O
μ	fluid dynamic viscosity (Pa s)
ρ	fluid density (kg/m^3)
σ	non-dimensional distance from wall of inner cylinder y/g
τ_{S_I}	axial component of shear stress on the surface of the inner cylinder (Pa)
τ_{S_O}	axial component of shear stress on the surface of the outer cylinder (Pa)
ϕ	azimuthal location with respect to inner cylinder
ψ	stream function (m^3/s)

* Corresponding author. Tel.: +44-1517944805; fax: +44-1517944848.
E-mail address: escudier@mechnet.liv.ac.uk (M.P. Escudier).

0142-727X/00/$ - see front matter
PII: S0142-727X(99)00059-4

$\bar{\psi}$ non-dimensional stream function ψ/Q
ω angular velocity of inner cylinder (rad/s)

1. Introduction

In the absence of inner cylinder rotation, the effect of eccentricity ε on fully developed laminar flow of a Newtonian fluid through an annulus is to produce a flow in which the peak velocity increases progressively with azimuthal location ϕ from the narrowest to the widest part of the annulus. The calculations of Tiedt (1966, 1967), as partially reported by Shah and London (1978), show that for a given radius ratio κ, this change in the velocity distribution $u(r,\phi)$ leads to a monotonic decrease in $f \cdot Re$ with ε, where f is the Fanning friction factor and Re the bulk Reynolds number.

The flow generated in an annulus due to rotation of the inner cylinder in the absence of bulk axial flow is one of the most widely investigated topics in fluid mechanics. Of the hundreds of papers published to date, the majority have been concerned with the Taylor vortices which arise above a critical Taylor number Ta_C. Lockett (1992) showed that the occurrence of Taylor vortices is inhibited by eccentricity of the inner cylinder, his numerical calculations being confirmed by the recent experimental work of Escudier and Gouldson (1997) as well as by earlier experiments reported by Kamal (1966), Cole (1968), Vohr (1968) and Castle and Mobbs (1968). The flow separation and the recirculating eddy or vortex which occurs above a critical eccentricity for a given radius ratio have also received widespread attention (Kamal, 1966; Ballal and Rivlin, 1976; San Andres and Szeri, 1984; Ho Tung et al., 1993; Siginer and Bakhtiyarov, 1998). As we shall show, although this radial/tangential motion is independent of the axial component of velocity, it has a very strong influence on the axial velocity distribution when there is a bulk axial flow, particularly for the case of high eccentricity.

Relatively little has been published for bulk axial flow through an annulus with both eccentricity and rotation of the inner cylinder which is the subject of the present paper. Takeuchi and Jankowski (1982) and Lockett (1992) have demonstrated that the onset of Taylor vortices is delayed to higher Taylor numbers by bulk axial flow and we limit ourselves here to subcritical flows. The recent numerical work of Manglik (1998) and the analytical, numerical and experimental study of Ooms and Kampman-Reinhartz (1996), primarily

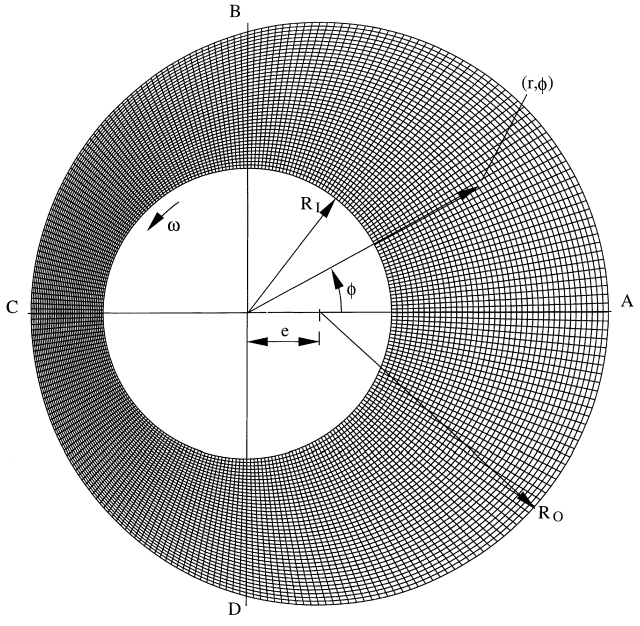

Fig. 1. Annulus geometry and computational grid 3 (40×256 cells) for radius ratio $\kappa = 0.5$ and eccentricity $\varepsilon = 0.5$.

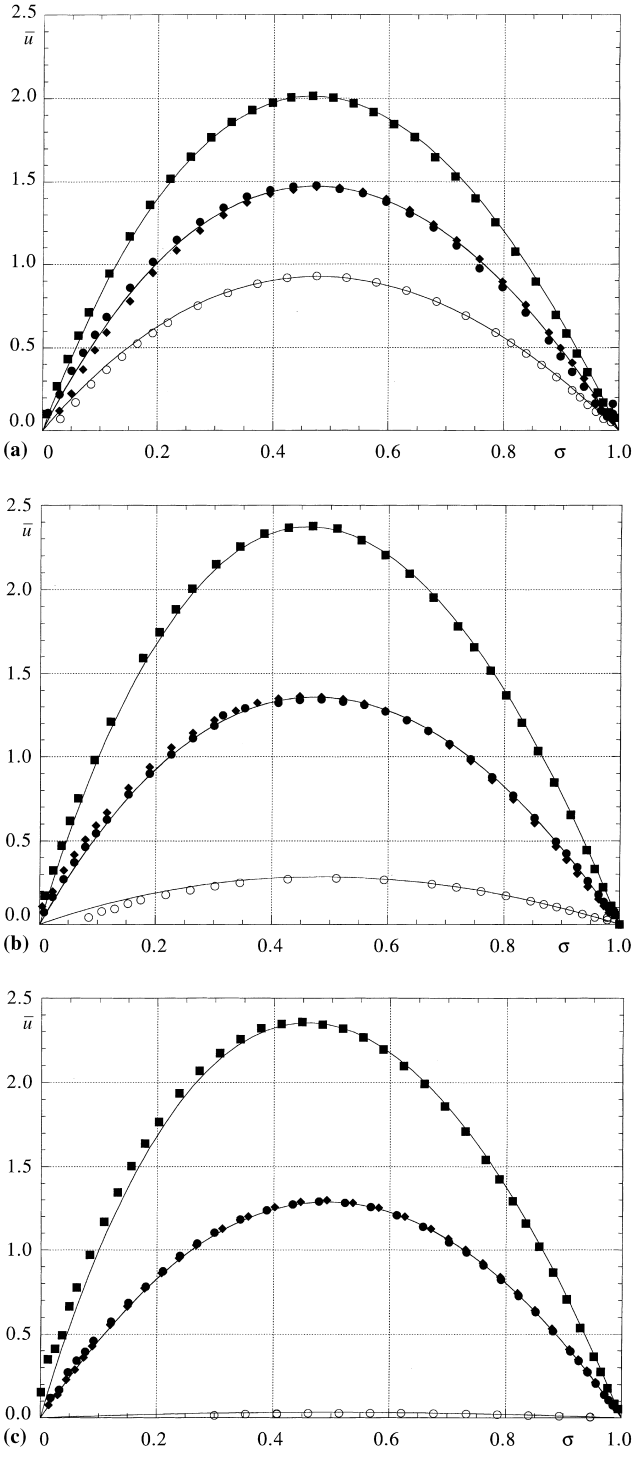

Fig. 2. Comparison between calculated and measured axial velocity distributions $\bar{u}(\sigma)$ for Reynolds number $Re = 105$ and no rotation with increasing eccentricity: (a) $\varepsilon = 0.2$; (b) $\varepsilon = 0.5$; (c) $\varepsilon = 0.8$. ■ Sector A; ● Sector B; ○ Sector C; ◆ Sector D.

concerned with the influence of rotation and eccentricity on the frictional pressure drop in annular flow, are the closest we are aware of to the present work and we shall refer to their results later in the paper. Another recent paper by Meuric et al. (1998) discusses a numerical study of the flow of both Newtonian and viscoplastic fluids in an eccentric annulus with inner cylinder rotation which leads to results for the former case consistent with those presented here.

In non-dimensional cylindrical coordinates centred on the axis of the inner cylinder, the equations to be solved for fully developed flow are

$$T\left(\bar{w}\frac{\partial\bar{w}}{\partial\bar{r}}+\frac{\bar{v}}{\bar{r}}\frac{\partial\bar{w}}{\partial\phi}-\frac{\bar{v}^2}{\bar{r}}\right)=-\frac{\partial\bar{p}}{\partial\bar{r}}+\frac{\partial}{\partial\bar{r}}\left(\frac{1}{\bar{r}}\frac{\partial}{\partial\bar{r}}\left(\bar{r}\bar{w}\right)\right)+\frac{1}{\bar{r}^2}\frac{\partial^2\bar{w}}{\partial\phi^2}-\frac{2}{\bar{r}^2}\frac{\partial\bar{v}}{\partial\phi},$$

$$T\left(\bar{w}\frac{\partial\bar{v}}{\partial\bar{r}}+\frac{\bar{v}}{\bar{r}}\frac{\partial\bar{v}}{\partial\phi}+\frac{\bar{v}\bar{w}}{\bar{r}}\right)=\frac{-1}{\bar{r}}\frac{\partial\bar{p}}{\partial\phi}+\frac{\partial}{\partial\bar{r}}\left(\frac{1}{\bar{r}}\frac{\partial}{\partial\bar{r}}\left(\bar{r}\bar{v}\right)\right)+\frac{1}{\bar{r}^2}\frac{\partial^2\bar{v}}{\partial\phi^2}+\frac{2}{\bar{r}^2}\frac{\partial\bar{w}}{\partial\phi},$$

$$T\left(\bar{w}\frac{\partial\bar{u}}{\partial\bar{r}}+\frac{\bar{v}}{\bar{r}}\frac{\partial\bar{u}}{\partial\phi}\right)=\frac{1}{2}f\cdot Re+\frac{1}{\bar{r}}\frac{\partial}{\partial\bar{r}}\left(\bar{r}\frac{\partial\bar{u}}{\partial\bar{r}}\right)+\frac{1}{\bar{r}^2}\frac{\partial^2\bar{u}}{\partial\phi^2},$$

$$\frac{\partial}{\partial\bar{r}}\left(\bar{r}\bar{w}\right)+\frac{\partial\bar{v}}{\partial\phi}=0$$

subject to the boundary conditions

$$\bar{u}=\bar{v}=\bar{w}=0 \quad \text{on the outer cylinder,}$$
$$\bar{w}=0,\quad \bar{v}=1,\quad \bar{u}=0 \quad \text{on the inner cylinder.}$$

The non-dimensional variables are defined by

$$\bar{w}\equiv\frac{w}{\omega R_{\mathrm{I}}},\quad \bar{v}\equiv\frac{v}{\omega R_{\mathrm{I}}},\quad \bar{u}\equiv\frac{u}{U},\quad \bar{r}\equiv\frac{r}{\delta},\quad \bar{p}\equiv\frac{p\delta}{\mu\omega R_{\mathrm{I}}},$$

and the parameters T, f and Re by

$$T\equiv\frac{\rho\omega R_{\mathrm{I}}\delta}{\mu},\quad f\equiv-\frac{\delta}{\rho U^2}\frac{\partial p}{\partial z}\ \text{(i.e. Fanning friction factor)},$$
$$Re\equiv\frac{2\rho U\delta}{\mu}.$$

For consistency with previous work, we shall present the results in terms of the Taylor number Ta rather than T where

$$Ta\equiv\left(\frac{\rho\omega}{\mu}\right)^2 R_{\mathrm{I}}\delta^3=\frac{\delta T^2}{R_{\mathrm{I}}}=\left(\frac{1}{\kappa}-1\right)T^2$$

with

$$\kappa\equiv\frac{R_{\mathrm{I}}}{R_{\mathrm{O}}}\quad\text{and}\quad\delta\equiv R_{\mathrm{O}}-R_{\mathrm{I}}.$$

As is evident, the equations for $\bar{v}$ and $\bar{w}$ for fully developed flow are independent of $\bar{u}$ and in principle can be solved separately. An outline of the method used to carry out the numerical calculations is given in Section 2. In Section 3 we report on comparisons with the analytical $f\cdot Re$ values of Tiedt (1966, 1967) and the numerical calculations of Manglik and Fang (1995) for the situation of no inner cylinder rotation. The code is also validated against the experimental data of Escudier and Gouldson (1997) for bulk flow both with rotation and with no rotation of the inner cylinder. In Section 4 of the paper we present the results of extensive numerical calculations for the influence on fully developed flow through an annulus of radius ratio κ, eccentricity ε and Taylor number Ta.

Although this paper is concerned with the flow of a Newtonian fluid, the practical motivation for the work is its relevance to the flow of drilling mud in an oil or gas wellbore during drilling operations. The mud is pumped down the rotating drillpipe and returned to the surface mud pit through the annulus between the drillpipe and the wellbore wall. The drilling mud has to satisfy several different requirements, including cooling and lubricating the drillbit, cleaning the workface, carrying drilled cuttings to the surface, preventing ingress of formation fluids into the wellbore, and preventing wellbore collapse. As a consequence of the multiplicity of operational requirements, the rheology of a drilling mud is generally non-Newtonian in character (Alderman et al., 1988): almost invariably shear thinning, and often exhibiting viscoelastic and thixotropic properties as well as a yield stress. In addition to the complex rheological nature of the liquid itself, drilling mud is usually contaminated by rock cuttings and formation fluids. Operational constraints in wells of great depth or extended reach, particularly the need to limit mud pressure to avoid fracturing the rock surrounding the borehole, often restrict the flow of a drilling mud in the annulus (usually eccentric to an uncontrolled and unknown extent) to the laminar regime (Ooms and Kampman-Reinhartz, 1996). Such flows thus represent a relatively rare example of laminar flows with major industrial relevance. It is also the case that the length-to-diameter ratio of a wellbore more than warrants the assumption of fully developed flow. The radius ratio of 0.506 adopted in the experimental work of Escudier and Gouldson (1997), against which we partially validate our numerical calculations, is typical of conventional drilling.

2. Outline of the numerical procedure

The continuity and momentum equations for three-dimensional, incompressible Newtonian fluid flow were

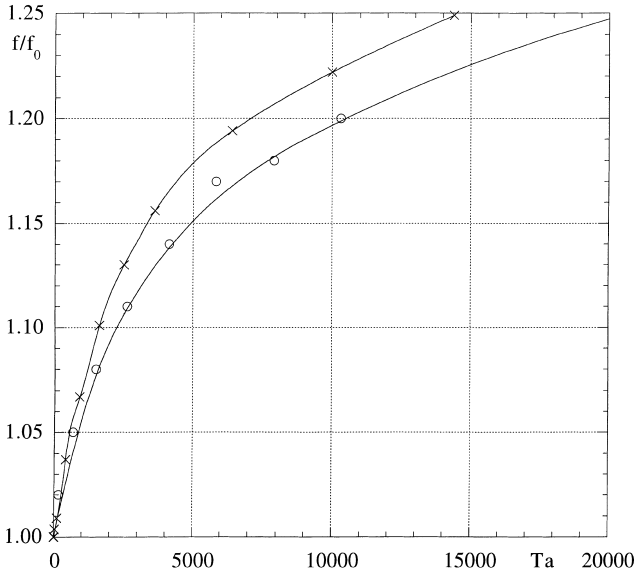

Fig. 3. Comparison between computed ratio of friction factors with and without rotation f/f_0 and experimental data of Ooms and Kampman-Reinhartz (1996) (—○—) for radius ratio $\kappa=0.5$ and eccentricity $\varepsilon=0.5$. Calculations of Ooms and Kampman Reinhartz (—x—).

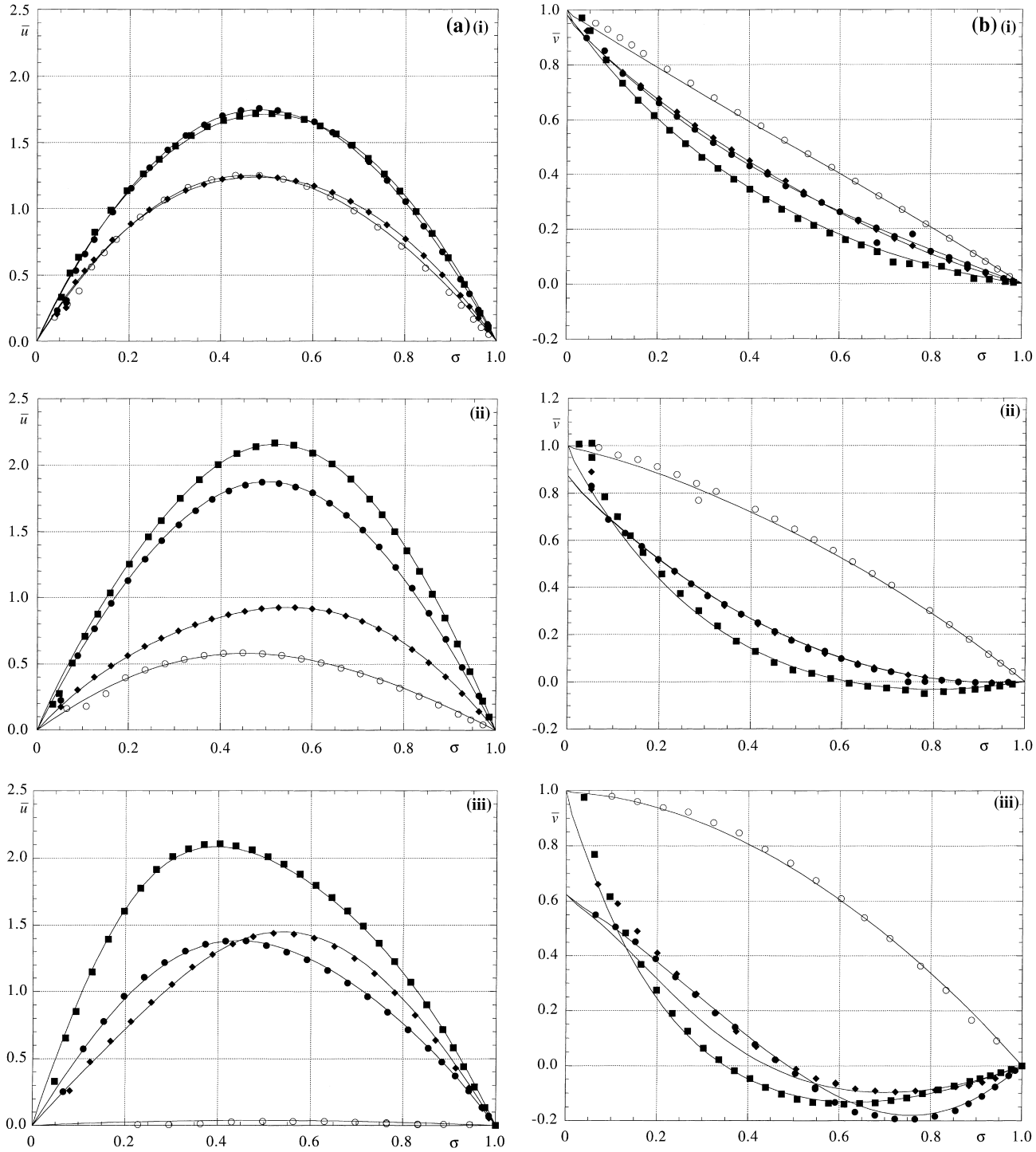

Fig. 4. Comparison between calculated and measured velocity distributions for Taylor number $Ta \approx 3000$ and increasing eccentricity: (a) axial velocity component $\bar{u}(\sigma)$; (b) tangential velocity component $\bar{v}(\sigma)$; (i) $\varepsilon = 0.2$; (ii) $\varepsilon = 0.5$; (iii) $\varepsilon = 0.8$. Symbols as for Fig. 2.

Table 1
Reynolds and Taylor numbers for experiments of Escudier and Gouldson (1997)

Figure no.	ε	Re	Ro	Ta	$U/\omega R_I$
4(a) (i) and 4 (b) (i)	0.2	105	55	2700	1.00
4 (a) (ii) and 4 (b) (ii)	0.5	115	47	3000	1.03
4 (a) (iii) and 4 (b) (iii)	0.8	120	56	2900	1.08

transformed into a general, non-orthogonal coordinate system for calculating the Cartesian velocity components. These equations were then discretised following the finite-volume approach of Patankar (1980), but adapted for collocated, non-orthogonal grids, as described in Peric (1985) and Oliveira (1992). The calculations were carried out using a second order central differencing scheme and the deferred correction approach was used in order to ensure numerical stability for the convective terms. The solution algorithm was a modified version of the SIMPLEC algorithm of van Doormal and Raithby (1984) adapted for time marching as explained in Issa and Oliveira (1994) where details can be found of the particular procedure used to evaluate mass fluxes at cell faces.

The coordinate system was centered at the inner cylinder axis and the three-dimensional annular geometry represented by 16 structured blocks around the annulus. A cross section of the annular geometry and the grid arrangement for a typical numerical calculation are shown in Fig. 1. Since the fully developed flow condition was of concern here, only one row of cells ($\approx D_H$ in length) was needed in the axial direction and the procedure of Patankar and Spalding (1972) was adopted to correct the axial pressure gradient $\partial\bar{p}/\partial\bar{z}$. A systematic grid refinement study was performed using three progressively finer uniform grids: 10×64, 20×128 and (as shown in Fig. 1) 40×256. These grids were uniform in the sense that at each angular position the radial width of the cells was constant and at each radial position the angular width was also constant. The solutions produced using the three meshes were then improved by two successive applications of Richardson's extrapolation technique (Ferziger, 1983), which produced fourth order accurate values for $f \cdot Re$.

In the concentric case the calculated values of $f \cdot Re$ are within 0.005% of the exact (analytical solution) values. For the eccentric situation there is no complete analytical solution [1] but an indication of the numerical uncertainty was achieved by comparing the results of calculations for both $\varepsilon = 0.5$ and $\varepsilon = 0.95$ with those estimated by applying Richardson's extrapolation three times, i.e. using results from the three meshes and a fourth finer grid, the result of which is here assumed to represent the exact value. This procedure resulted in discrepancies in $f \cdot Re$ of 0.05% and 0.002%, respectively. We assume that for all cases considered here the application of Richardson's extrapolation technique to identical levels provides similarly accurate approximations to the exact value.

3. Code validation

As can be seen from Fig. 2, the results of calculations for $\varepsilon = 0.2$, 0.5 and 0.8 and $\kappa = 0.506$ for zero rotation of the inner cylinder are in excellent agreement with the velocity-profile data of Escudier and Gouldson (1997) obtained using a high-precision laser Doppler anemometer (LDA).

The mass flowrate used to determine the value of U for the normalisation of the experimental velocity distributions was measured independently and required minor corrections (between 1.4% and 4.2%) to ensure that overall mass conservation was satisfied. Uncertainties in the locations of the inner cylinder and the LDA probe volume necessitated corrections of between 0.1 and 1.0 mm to the gap width to ensure that the measured velocity distribution correctly approached the velocity of the inner cylinder. The calculated results are indis-

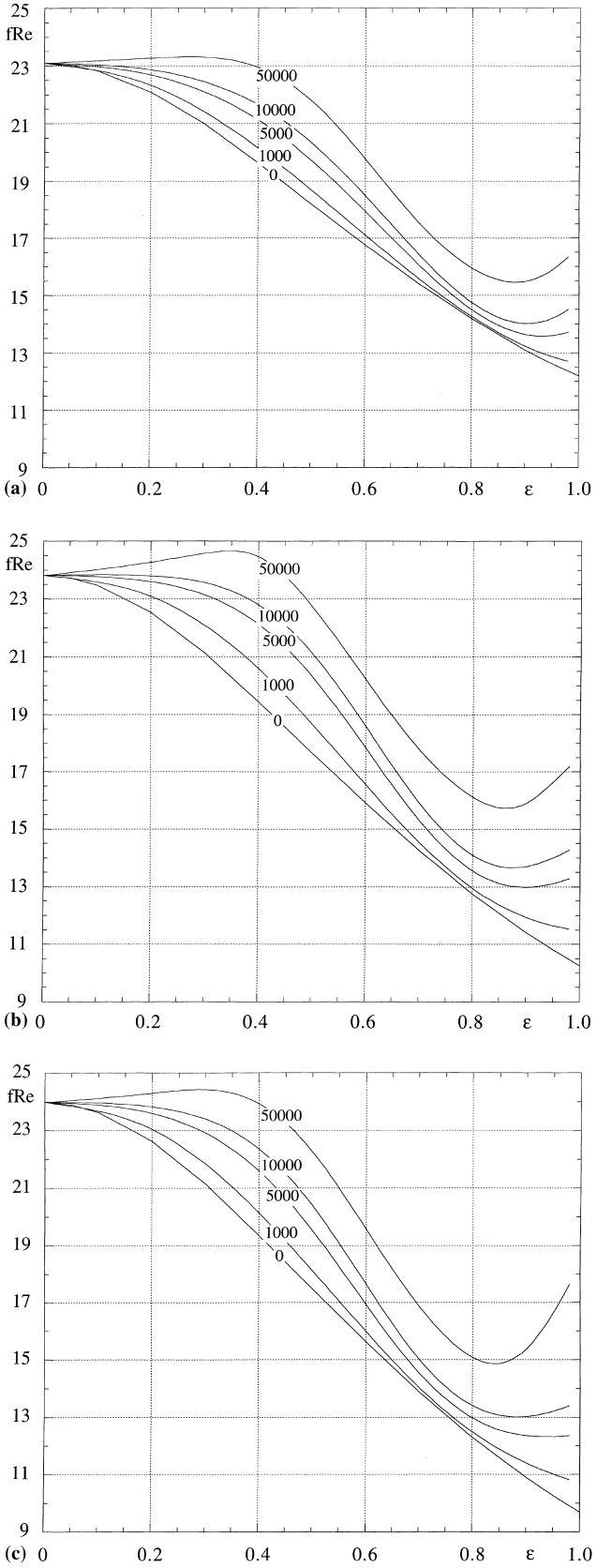

Fig. 5. Variation of frictional pressure loss $f \cdot Re$ with eccentricity ε for increasing Taylor number Ta (parameter on curves) and radius ratio κ: (a) $\kappa = 0.2$; (b) $\kappa = 0.5$; (c) $\kappa = 0.8$.

[1] Ooms and Kampman-Reinhartz (1996) give an analytical solution based on a perturbation analysis which is restricted to small values of the perturbation parameters but which demonstrates the crucial role of inertia in annular flows with centrebody rotation.

Table 2
Computed variation of frictional pressure loss $f \cdot Re$ with radius ratio κ, Taylor number Ta and eccentricity ε (values for $Ta = 0$, $\kappa = 0.2$ and 0.8, $\varepsilon \neq 0.98$, from Tiedt, 1967)

$\kappa = 0.2$						
Ta	$\varepsilon = 0.2$	0.3	0.4	0.5	0.6	0.7
0	22.093	20.985	19.641	18.197	16.760	15.407
100	22.125	21.039	19.706	18.256	16.803	15.431
1000	22.327	21.397	20.151	18.682	17.111	15.587
2500	22.518	21.758	20.638	19.181	17.498	15.800
5000	22.688	22.096	21.124	19.717	17.945	16.068
10 000	22.860	22.449	21.655	20.332	18.491	16.438
50 000	23.267	23.303	22.943	21.788	19.775	17.547
Ta	0.8	0.85	0.9	0.95	0.98	
0	14.181	13.625	13.105	12.625	12.356	
100	14.193	13.636	13.124	12.657	12.400	
1000	14.255	13.699	13.235	12.874	12.712	
2500	14.350	13.799	13.407	13.184	13.148	
5000	14.493	13.952	13.640	13.598	13.714	
10 000	14.741	14.222	14.019	14.195	14.497	
50 000	15.944	15.540	15.486	15.879	16.335	
$\kappa = 0.5$						
Ta	$\varepsilon = 0.2$	0.3	0.4	0.5	0.6	0.7
0	22.517	21.117	19.439	17.655	15.895	14.244
100	22.629	21.282	19.619	17.804	15.993	14.292
1000	23.088	22.091	20.605	18.686	16.560	14.545
2500	23.396	22.703	21.454	19.555	17.196	14.879
5000	23.600	23.140	22.137	20.344	17.849	15.308
10 000	23.800	23.568	22.804	21.149	18.603	15.917
50 000	24.277	24.585	24.470	22.758	20.236	17.782
Ta	0.8	0.85	0.9	0.95	0.98	
0	12.745	12.059	11.414	10.811	10.468	
100	12.780	12.106	11.489	10.929	10.618	
1000	12.956	12.375	11.944	11.649	11.539	
2500	13.207	12.713	12.449	12.383	12.416	
5000	13.558	13.126	12.994	13.119	13.287	
10 000	14.093	13.709	13.703	14.005	14.275	
50 000	16.115	15.744	15.893	16.631	17.188	
$\kappa = 0.8$						
Ta	$\varepsilon = 0.2$	0.3	0.4	0.5	0.6	0.7
0	22.631	21.146	19.367	17.480	15.622	13.882
100	22.687	21.238	19.468	17.559	15.667	13.901
1000	23.041	21.834	20.149	18.121	15.989	14.038
2500	23.344	22.405	20.878	18.786	16.408	14.243
5000	23.597	22.912	21.602	19.527	16.933	14.540
10 000	23.824	23.400	22.361	20.396	17.650	15.018
50 000	24.298	24.425	23.936	22.258	19.573	16.872
Ta	0.8	0.85	0.9	0.95	0.98	
0	12.304	11.581	10.903	10.277	9.859	
100	12.328	11.623	10.975	10.381	10.049	
1000	12.489	11.892	11.405	11.016	10.823	
2500	12.701	12.192	11.858	11.645	11.567	
5000	12.981	12.566	12.364	12.325	12.360	
10 000	13.403	13.073	13.028	13.216	13.396	
50 000	15.078	14.865	15.383	16.642	17.644	

tinguishable from those of Manglik (1996) which are based upon the numerical solutions reported by Manglik and Fang (1995) for the fully developed flow equations. We conclude that for the situation without rotation the results of the code converge to the solution for the fully developed state.

The validity of our results for the non-rotating case was also evident from comparisons of values of $f \cdot Re$ with the exact analytical solutions of Tiedt (1966, 1967) where the agreement in all cases was within 0.13% whereas Manglik and Fang's (1995) results show an increasing discrepancy with increasing ε and decreasing κ, to values as high as -3.7% for $\varepsilon = 0.6$, $\kappa = 0.5$ and -13.7% for $\varepsilon = 0.6$, $\kappa = 0.25$ (Manglik and Fang reported no results for higher values of ε). Manglik and Fang attribute the increasing numerical errors with in-

creasing ε and decreasing κ to a lack of orthogonality in their mesh.

In Fig. 3 we validate our calculations for the influence of rotation on frictional pressure drop against the data of Ooms and Kampman-Reinhartz (1996) for $\varepsilon = 0.5$, $\kappa = 0.5$. As in their paper, we present the results in the form of the ratio of $f \cdot Re$ to the value for $Ta = 0$ (i.e. f/f_0). The level of agreement with the experimental data is clearly very good and far better than for the curve representing the calculations of Ooms and Kampman-Reinhartz.

In Fig. 4(a) and (b) we compare our calculations with the measured velocity profiles of Escudier and Gouldson (1997) for $Ta \approx 3000$ which corresponds to $U/\omega R_I \approx 1$. The exact values of the parameters for these experiments are listed in Table 1. As with the case for $Ta = 0$, the agreement for the axial component of velocity is exceptionally good whilst the discrepancies for the tangential component are small and attributable to the experiments rather than the numerical calculations. We shall discuss in more detail later the calculated flow behaviour, but note at this point that with increasing eccentricity the axial velocity distributions are increasingly distorted due to the inner cylinder rotation: the positions of the peak velocities in the wide and narrowing gaps (sectors A and B) move towards the inner cylinder whilst that for the widening gap (sector D) moves outward. These changes in profile shape are responsible for increases in the $f \cdot Re$ values and, as will be seen shortly, eventually dominate over the tendency for $f \cdot Re$ to decrease with increasing eccentricity. Both the experimental data and the numerical calculations confirm the occurrence of separation, reattachment and recirculation in the crossflow plane found previously in the absence of bulk throughflow by Kamal (1966), Ballal and Rivlin (1976), San Andres and Szeri (1984) and Siginer and Bakhtiyarov (1998).

4. Results of numerical calculations

Detailed calculations have been carried out for radius ratios of 0.2, 0.5 and 0.8 covering eccentricities up to 0.98 and Taylor numbers up to 50 000. The principal outcome of this investigation is represented by the variations in $f \cdot Re$ with κ, ε and Ta shown in Fig. 5 and tabulated in Table 2. The results for $\kappa = 0.5$ are also given in Fig. 6 in the form f/f_0 where f_0 indicates the value of f for zero rotation, all other factors remaining the same. For a given radius ratio, as the Taylor number is increased from zero, the value of $f \cdot Re$ at any eccentricity is increased with the relative increase (above the values for $Ta = 0$) passing through a maximum for $\varepsilon \approx 0.5$ and a minimum for $\varepsilon \approx 0.75$ (Fig. 5). An unexpected feature of the results is that for Taylor numbers in excess of about 5000, the $f \cdot Re$ values fall to a minimum for $\varepsilon \approx 0.9$ and then show an increase, a trend which has not been revealed in previous experimental and theoretical work. Some of the changes in $f \cdot Re$ are in fact evident in the numerical calculations reported by Ooms and Kampman-Reinhartz (1996) though they conclude that f passes through a maximum (at $\varepsilon \approx 0.5$ for $\kappa = 0.6$ and $Ta = 1800$) and then decreases with increase in ε even though their perturbation analysis reveals a minimum in f/f_0 at $\varepsilon \approx 0.75$. Manglik's (1998) calculations suggest that $f \cdot Re$ reaches an asymptote as ε approaches one but, as reported by Manglik and Fang (1995), due to their grid configuration the results are subject to increasing numerical error as ε increases above about 0.8.

To assist in the interpretation of the results for $f \cdot Re$ we shall refer to the corresponding crossflow streamlines, to the distributions of axial velocity and the shear stress on the surfaces of the inner and outer cylinders, and to the tangential flowrate. Since the qualitative influence of ε and Ta on $f \cdot Re$ for $\varepsilon < 0.8$ is the same for each of the three radius ratios for which calculations were performed, we shall base the discussion on the results for $\kappa = 0.5$. The detailed flow behaviour for $\kappa = 0.2$ is significantly different from that for $\kappa = 0.5$ and 0.8 at eccentricities above about 0.8 and is discussed separately. Axial velocity isovels and crossflow streamlines for $\kappa = 0.5$ and $Ta = 4200$ covering eccentricities of 0.2, 0.7 and 0.95 are shown in Fig. 7 and the corresponding distributions of the axial component of the shear stress for the full range of ε in Fig. 10.

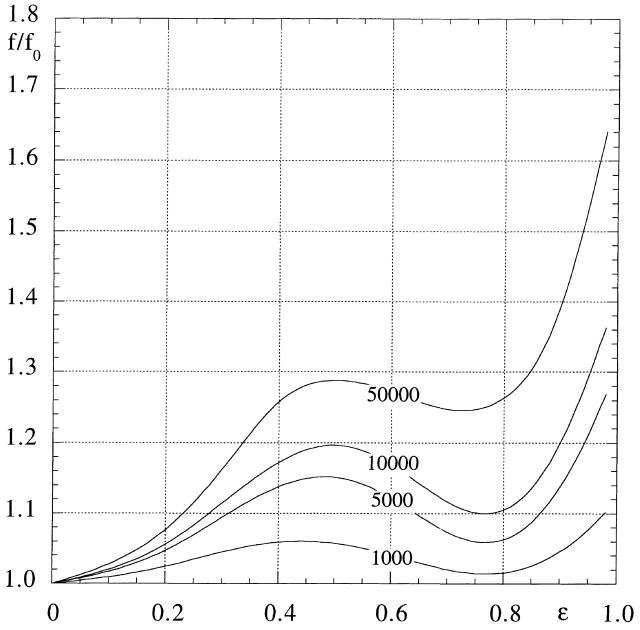

Fig. 6. Variation of ratio of friction factor with and without rotation f/f_0 with eccentricity ε and Taylor number Ta (parameter on curves) for radius ratio $\kappa = 0.5$.

For a fixed rotation speed, at low eccentricity (up to about 0.3) the crossflow streamlines are slightly distorted (Fig. 7 (a)) and tangential flow around the annulus is slightly reduced by the blockage effect associated with the eccentricity, thereby countering the tendency for the axial velocity peak to move in the sense of rotation into the narrowing gap. There is also a slight radial displacement of the axial velocity peak towards the inner cylinder which, in contrast to the angular displacement, increases with the eccentricity. As the eccentricity is increased above about 0.3, recirculation of the crossflow develops adjacent to the surface of the outer cylinder and is roughly centred in the wide gap. With further increase in ε the recirculation occupies an increasing fraction of the annulus and increasingly inhibits the tendency for fluid with high axial momentum to be swept into the narrowing gap. Once ε exceeds 0.7, the recirculation has spread to such an extent (Fig. 7 (b)) that the angular displacement of the axial velocity peak is reduced to near zero and then becomes increasingly negative as ε is further increased (Fig. 7 (c)). Although we have highlighted the displacement of the velocity peak, the entire flowfield is increasingly distorted as the eccentricity and Taylor number are increased with the magnitude of the axial velocity maximum progressively decreasing with increasing Ta whereas the angular and radial displacements progressively increase at any given eccentricity. The magnitude of the peak axial velocity passes through a maximum for $\varepsilon \approx 0.6$ (there is a slight influence of Ta and a greater one of κ) when it is located in the wide gap.

An unexpected feature of the calculations for radius ratios of 0.5 and 0.8, but not seen for $\kappa = 0.2$, is the appearance of a

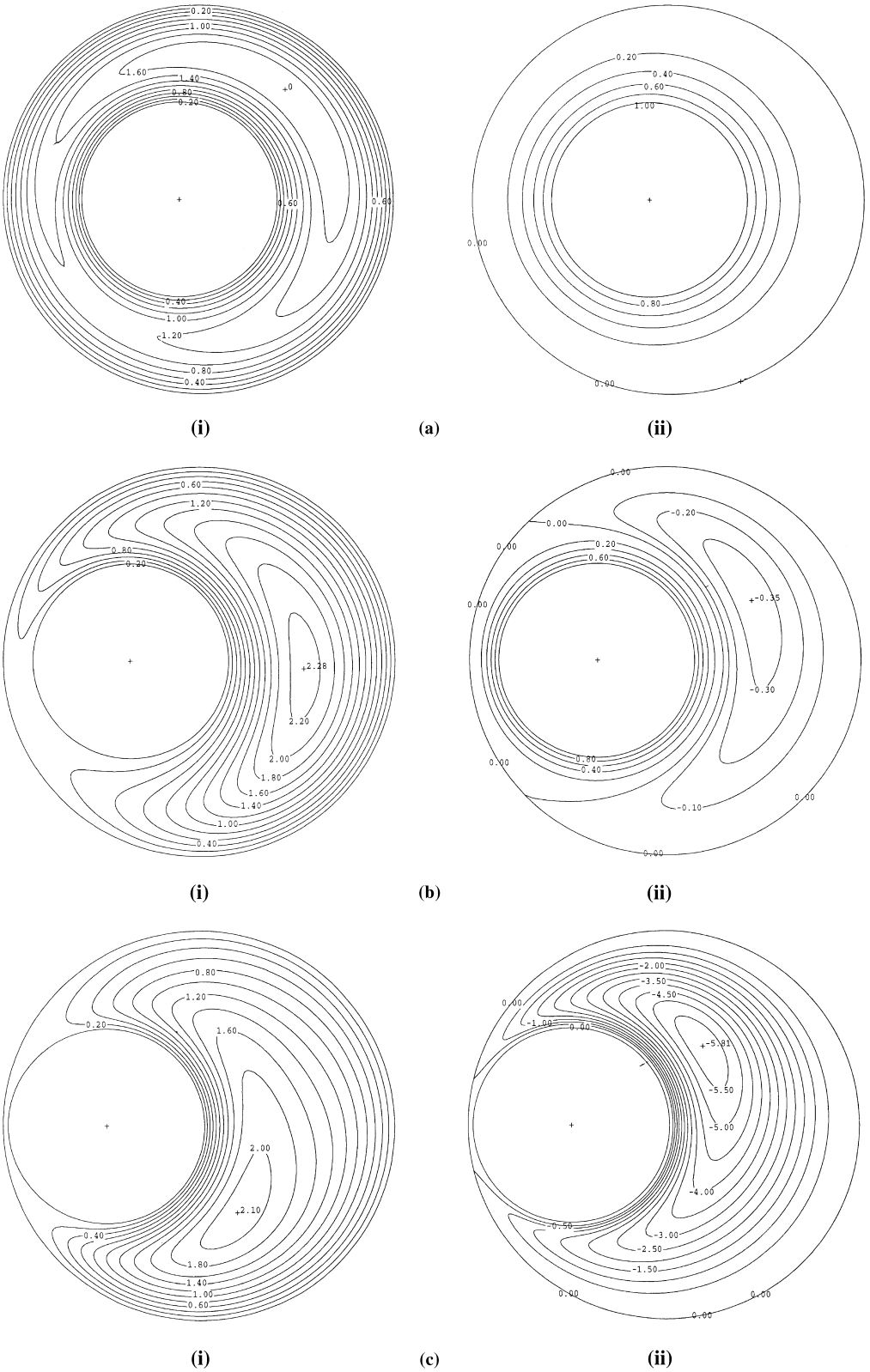

Fig. 7. (i) Axial velocity isovels $\bar{u}(\bar{r},\phi)$ and (ii) crossflow streamlines $\bar{\psi}(\bar{r},\phi)$ for radius ratio $\kappa = 0.5$ and Taylor number $Ta = 4200$ for increasing eccentricity (a) $\varepsilon = 0.2$; (b) $\varepsilon = 0.7$; (c) $\varepsilon = 0.95$.

second peak in the axial velocity, located in the narrowing gap, for combinations of very high eccentricities and Taylor numbers. For example, for $\kappa = 0.5$ a second peak is found for $\varepsilon = 0.98$ and $Ta = 10\,000$, for $\varepsilon = 0.9$ and $Ta = 25\,000$, and for $\varepsilon = 0.85$ and $Ta = 50\,000$. The emergence and growth of the second peak is illustrated in Fig. 8 for $\kappa = 0.5$, $Ta = 50\,000$,

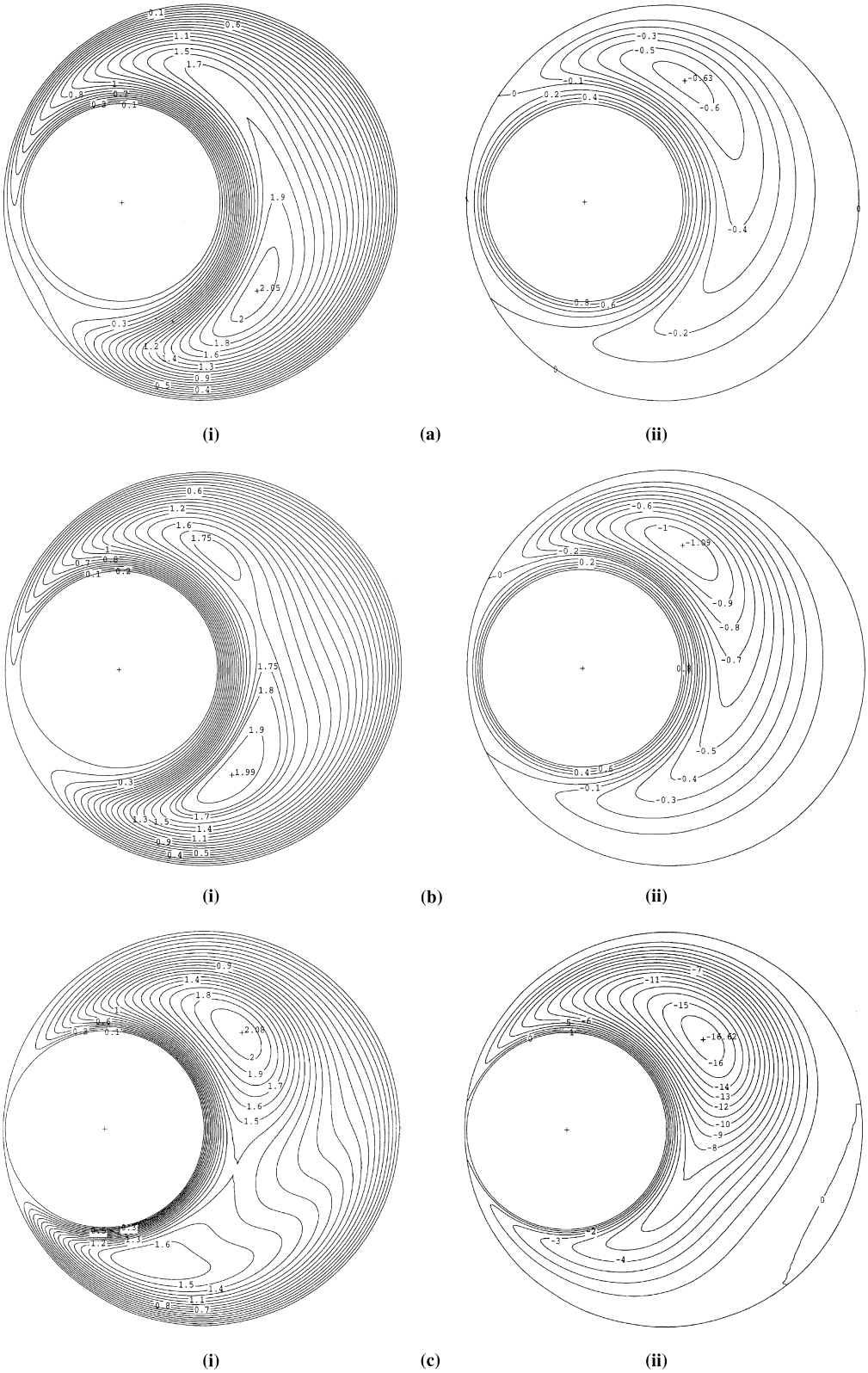

Fig. 8. (i) Axial velocity isovels $\bar{u}(\bar{r},\phi)$ and (ii) crossflow streamlines $\bar{\psi}\ (\bar{r},\phi)$ for radius ratio $\kappa = 0.5$ and high Taylor number $Ta = 50000$ at high values of eccentricity (a) $\varepsilon = 0.8$; (b) $\varepsilon = 0.85$; (c) $\varepsilon = 0.98$.

$\varepsilon = 0.8$, 0.85 and 0.98. As can be seen from the crossflow streamlines, the location of the new axial velocity peak is practically coincident with the eye of the recirculating eddy which has also moved into the narrowing gap at these high values of ε and Ta. This second peak in the axial velocity becomes stronger than the first as ε is increased but located

further from the inner cylinder. Under these conditions a second region of recirculating crossflow emerges in the widening gap close to the surface of the outer cylinder (Fig. 8(c)). The behaviour for $\kappa = 0.2$ is quite different: no second maximum occurs and the peak in axial velocity moves back into the narrowing gap as Ta is increased, as can be seen in Fig. 9.

The distortions of the axial velocity distribution and the movement of the peak axial velocity, due to the combined effects of eccentricity and rotation result in the distributions of the axial component of the surface shear stress shown in Fig. 10 for $\kappa = 0.5$, $Ta = 4200$. In order to reveal the relative contributions to f, the shear stress on the surface of the inner cylinder τ_{S_I} has been weighted by R_I and that on the outer cylinder τ_{S_O} by R_O. The response of the distributions of both τ_{S_O} and τ_{S_I} to increased eccentricity is similar. Each initially has a maximum in the narrowing gap and a minimum in the widening gap. With increasing eccentricity the maxima move against the sense of rotation decreasing in magnitude until $\varepsilon \approx 0.75$ (τ_{S_I}) or 0.85 (τ_{S_O}) after which the magnitude increases. The minima also move against the sense of rotation towards the narrow gap and decrease monotonically to zero as ε approaches one. The distribution of τ_{S_I} remains roughly symmetrical with respect to ϕ as ε increases whereas τ_{S_O} is increasingly skewed towards the narrow gap. The increase in $f \cdot Re$ evident in Fig. 5 for the higher Taylor numbers as ε approaches one may be attributed to the increased levels of shear stress in the widening gap.

Caution needs to be exercised in assessing the results of the calculations reported here since it has been assumed throughout that the critical Taylor number has not been exceeded. Although both an imposed throughflow and eccentricity are known to increase the critical Taylor number for any given radius ratio the stability boundaries have yet to be calculated for the combinations of ε and κ we consider here. However, we note that the empirical expression given by Lockett (1992) yields a critical value of 80 000 for Ta as ε approaches one, well above the maximum value (50 000) considered here. In addition, transition to turbulence at high Taylor and Reynolds numbers must also limit the general validity of our results.

5. Concluding remarks

On the basis of the discussion of the various effects on $f \cdot Re$, it is convenient to separate the differences in flow behaviour for low, high and intermediate values of eccentricity.

For $\varepsilon < 0.3$ the flow is rotation dominated. $f \cdot Re$ remains approximately constant with ε, or may even increase above the non-rotating concentric value. The main effect here is for fluid to be dragged around the annulus by rotation of the inner cylinder thereby advecting the peak velocity from the wide gap into the narrowing gap. The axial gradient is increased in the vicinity of both the inner and outer cylinders thereby inducing higher values of $f \cdot Re$. The maxima in τ_{S_I} and τ_{S_O} for $\varepsilon < 0.3$ are located in the narrowing gap.

In the intermediate regime, $0.3 < \varepsilon < 0.8$, the curve of $f \cdot Re$ versus ε shows the "normal" (i.e. without rotation) trend of reduction in friction with increased eccentricity. In this regime the secondary recirculation progressively develops and begins to move the location of maximum axial velocity back into the wide gap (but still with $\phi > 0°$). The resulting effect is to generate axial-velocity isovels similar to those without rotation and hence result in a reduction with ε in the magnitude of the maxima in τ_{S_I} and τ_{S_O} and so of $f \cdot Re$.

The third regime ($0.8 < \varepsilon < 1$) is recirculation dominated and it is here that qualitatively new and unexpected behaviour is observed. The location of peak velocity is advected by the stronger recirculation into the widening gap region ($\phi < 0°$) and then, as the flow turns to close the recirculating eddy, is forced toward the "lower" surface of the inner cylinder. This produces high localised maxima of τ_{S_I} and then of τ_{S_O} (see Fig. 10 for $\phi < -90°$) which reduces the tendency for $f \cdot Re$ to

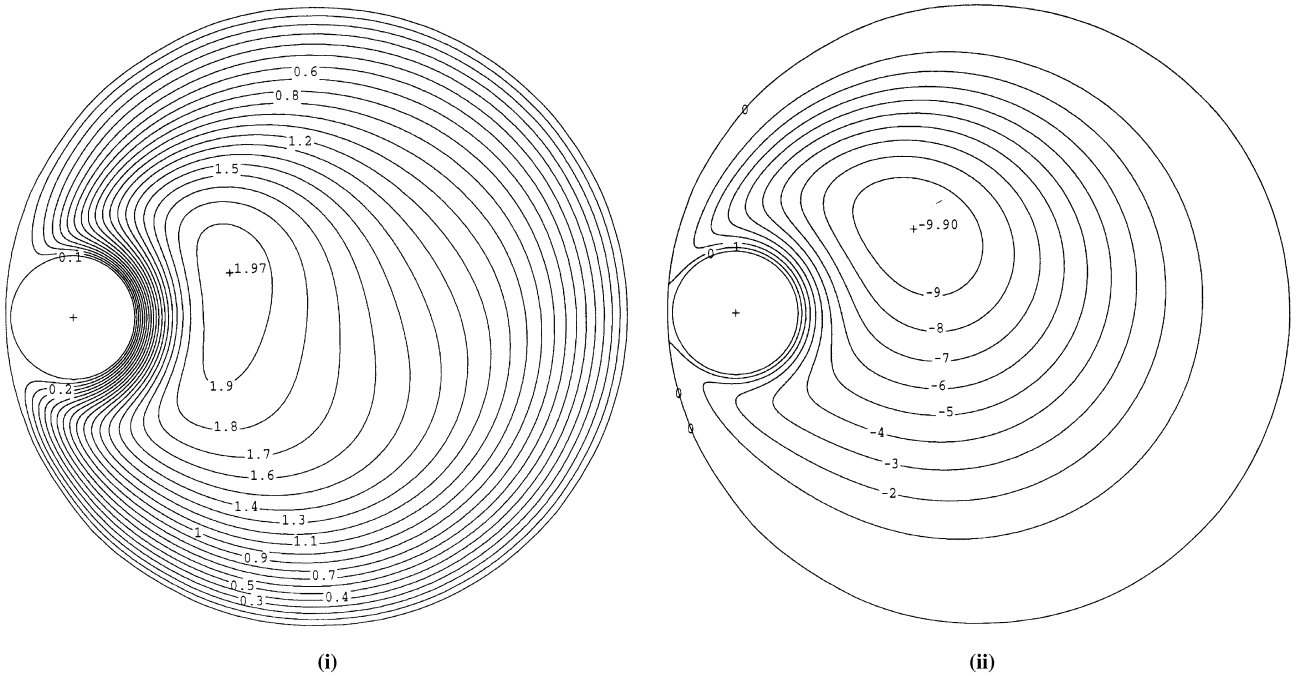

Fig. 9. (i) Axial velocity isovels $\bar{u}(\bar{r}, \phi)$ and (ii) crossflow streamlines $\bar{\psi}(\bar{r}, \phi)$ for small radius ratio $\kappa = 0.2$, high Taylor number $Ta = 50000$ and high eccentricity $\varepsilon = 0.98$.

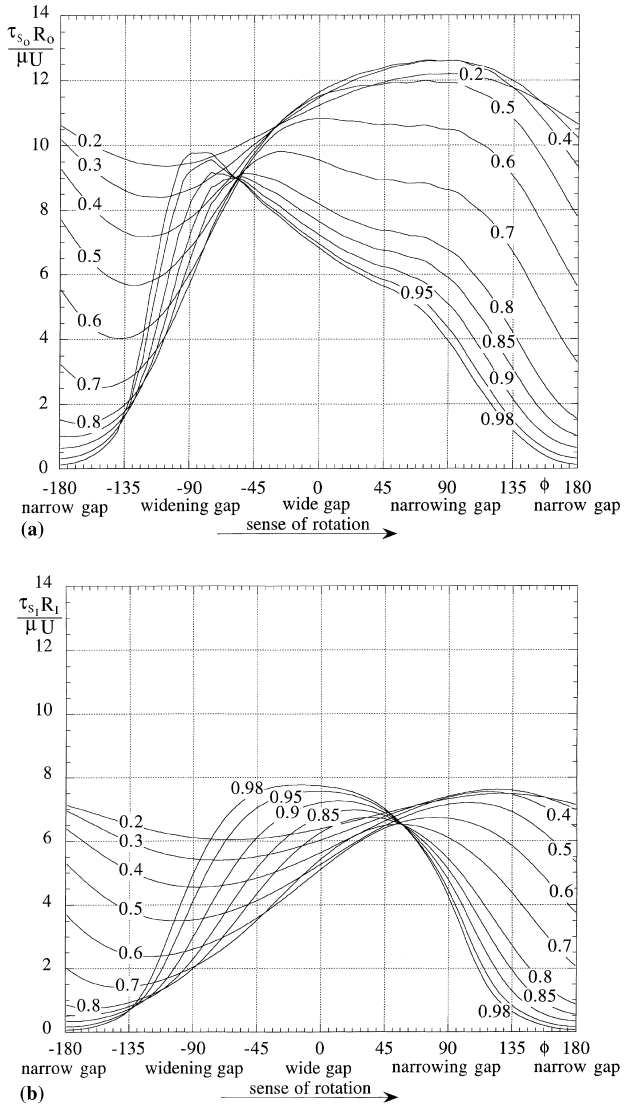

Fig. 10. Azimuthal distribution of surface shear stress for radius ratio $\kappa = 0.5$ and Taylor number $Ta = 4200$: (a) Outer cylinder $\tau_{S_O} R_O/\mu U$; (b) Inner cylinder $\tau_{S_I} R_I/\mu U$. Parameter on curves is eccentricity ε.

decrease with ε and eventually induces an increase. Indeed, for high Ta the axial velocity peak is so strongly advected towards the lower side of the inner cylinder, where it generates a strong rotation-directed layer, that two opposing effects act to create two local peaks of the axial velocity distribution with corresponding distortion of the isovels and an increase in $f \cdot Re$, neither feature observed hitherto either in calculations or experiments.

Acknowledgements

The financial support of EPSRC/MTD (research grant GR/F87813), Shell Research B.V. and British Gas plc is gratefully acknowledged by M.P. Escudier and I.W. Gouldson. P.J. Oliveira and F.T. Pinho acknowledge the receipt of a sabbatical leave grant from FCT (grants FMR/BSAB/68/98 and BLS 68/97 respectively). The authors' names are listed in alphabetical order.

References

Alderman, N.J., Ram Babu, D., Hughes, T.L., Maitland, G.C., 1988. The rheological properties of oil well drilling fluids. In: Proc. Xth Int. Cong. Rheology, Sydney, pp. 140–142.

Ballal, B.Y., Rivlin, R.S., 1976. Flow of a Newtonian fluid between eccentric rotating cylinders: Inertial effects. Arch. Rational Mech. Anal. 62, 237–294.

Castle, P., Mobbs, F.R., 1968. Hydrodynamic stability of the flow between eccentric rotating cylinders: Visual observations and torque measurements. In: Proc. IMechE, vol. 182, Part 3N. Tribology Convention.

Cole, J.A., 1968. Taylor vortices with eccentric rotating cylinders. Trans. ASME J. Lub. Technol., 285–296.

van Doormal, J.P., Raithby, G.D., 1984. Enhancements of the SIMPLE method for predicting incompressible fluid flows. Numer. Heat Transfer 7, 147–163.

Escudier, M.P., Gouldson, I.W., 1997. Effects of centrebody rotation on laminar flow through an eccentric annulus. In: Adrian, R.J., Durao, D.F.G., Durst, F., Heitor, M.V., Maeda, M., Whitelaw, J.H., (Eds.), Developments in Laser Techniques and Applications to Fluid Mechanics. Proc. Eighth Int. Symp., Lisbon, 1996. Springer, Berlin.

Ferziger, J.H., 1983. Numerical Methods for Engineering Application. Wiley, New York.

Ho Tung, J.N., Kleis, S.J., VanArsdale, W.E., 1993. The effect of polymer on azimuthal velocity profiles in an eccentric cylinder apparatus. In: Developments in Non-Newtonian Flows, vol. AMD–175, pp. 65–70.

Issa, R.I., Oliveira, P.J., 1994. Numerical predictions of phase separation in two-phase flow through T-junctions. Computers and Fluids 23, 347.

Kamal, M.M., 1966. Separation in the flow between eccentric cylinders. ASME J. Basic Eng., 717–724.

Lockett, T.J., 1992. Numerical simulation of inelastic non-Newtonian fluid flows in annuli. Ph.D. Thesis. Imperial College of Science, Technology and Medicine.

Manglik, R.M., 1996. Private communication.

Manglik, R.M., 1998. Private communication.

Manglik, R.M., Fang, P.P., 1995. Effects of eccentricity and thermal boundary conditions on laminar and fully developed flow in annular ducts. Int. J. Heat Fluid Flow 16 (4), 298–306.

Meuric, O.F.J., Wakeman, R.J., Chin, T.W., Fisher, K.A., 1998. Numerical flow simulation of viscoplastic fluids in annuli. Can. J. Chem. Eng. 76 (February), 27–39.

Oliveira, P.J., 1992. Computer modelling of multidimensional multiphase flow and application to T-junctions. Ph.D. Thesis. Imperial College of Science, Technology and Medicine.

Ooms, G., Kampman-Reinhartz, B.E., 1996. Influence of drill pipe rotation and eccentricity on pressure drop over borehole during drilling. Eur. J. Mech. B 15 (5), 695–711.

Patankar, S.V., 1980. Numerical Heat Transfer and Fluid Flow. Hemisphere, Bristol, PA, pp. 1–197.

Patankar, S.V., Spalding, D.B., 1972. A calculation procedure for heat, mass and momentum transfer in three-dimensional parabolic flows. Int. J. Heat Mass Transfer 15, 1787–1806.

Peric, M., 1985. A finite-volume method for the prediction of three-dimensional fluid flow in complex ducts. Ph.D. Thesis. Imperial College of Science, Technology and Medicine.

San Andres, A., Szeri, A.Z., 1984. Flow between eccentric rotating cylinders. ASME J. Appl. Mech. 51, 869–878.

Shah, R.K., London, A.L., 1978. Laminar flow forced convection in ducts. In: Advances in Heat Transfer. Academic Press, New York.

Siginer, D.A., Bakhtiyarov, S.I., 1998. Flow of drilling fluids in eccentric annuli. J. Non-Newt. Fluid Mech. 78, 119–132.

Takeuchi, D.I., Jankowski, D.F., 1982. A numerical and experimental investigation of the stability of spiral Poiseuille flow. J. Fluid Mech. 102, 101–126.

Tiedt, W., 1966. Berechnung des laminaren und turbulenten Reibungswiederstandes konzentrischer und exzentrischer Ringspalte. Part I.. Chem-Ztg, Chem. Appar. 90, 813–821.

Tiedt, W., 1967. Berechnung des laminaren und turbulenten Reibungswiederstandes konzentrischer und exzentrischer Ringspalte. Part II. Chem-Ztg, Chem. Appar. 91, 17–25.

Vohr, J.H., 1968. An experimental study of Taylor vortices and turbulence in flow between eccentric rotating cylinders. Trans. ASME J. Lub. Technol., 185–296.